nature communications

Article

https://doi.org/10.1038/s41467-025-62340-6

# Periplasmic protein quality control at atomic level in live cells

Received: 10 January 2025

Accepted: 17 July 2025

Published online: 24 September 2025

Check for updates

Lisandro J. González[1,2] ✉, Francisco J. Hita[1], Letizia Pontoriero[3], Roberta Pierattelli[3] ✉, Andres Binolfi[4,5] ✉ & Alejandro J. Vila[1,2,5] ✉

The periplasm of gram-negative bacteria facilitates critical functions, including nutrient uptake, cell wall metabolism, antibiotic resistance, and virulence. Efficient quality control of proteins involved in these processes is crucial for bacterial fitness and survival. The limited size of the periplasm has hindered high-resolution mechanistic investigations of complex processes within this compartment. Using in-cell NMR spectroscopy, we dissect the mechanism of periplasmic quality control of the metallo-β-lactamase NDM-1 under conditions of zinc starvation, which destabilizes its native structure promoting its degradation. We show that the protease Prc targets membrane-bound NDM-1 at specific residues and secondary structure motifs, while DegP processes peptides generated by Prc. This approach discloses the concerted mechanism of these proteases at atomic resolution in the periplasm of live cells.

The periplasm is a compartment confined by the inner and outer membrane of Gram-negative bacteria, acting as a sensory/responsive interface between the cell and environmental cues[1]. The periplasm is essential for bacterial survival and adaptability by providing structural integrity through the peptidoglycan, and by hosting critical processes such as nutrient uptake, secretion of virulence factors, signal transduction, and antibiotic resistance[2,3]. These functions are performed by proteins, which collectively enhance the ability of pathogens to establish infections, evade the host immune response and cause disease, making the periplasm a critical component of bacterial virulence[4]. The metabolic orchestration of these proteins hinges on their effective translocation from the cytoplasm, precise folding, and stringent protein quality control (PQC) mechanisms[5,6]. Understanding PQC is therefore essential for deciphering bacterial physiology, pathogenesis, and virulence. In contrast to the cytoplasm, the periplasm is separated from the extracellular milieu by a porous outer membrane. Thus, periplasmic proteins must endure variable, occasionally extreme, environmental conditions, requiring specific PQC mechanisms[5–7].

The periplasm represents ca. 10–20% of the total cell volume despite hosting almost one third of the bacterial proteome[8,9]. Its small size precludes achieving high-resolution mechanistic details by microscopy techniques in live cells. Thus, most of the knowledge on periplasmic process relies on biochemical or structural studies in vitro or on genetic studies interrogating the bacterial cell physiology. Here, we fill this gap by using in-cell NMR[10–15] to dissect the quality control mechanism of zinc-dependent, New Delhi Metallo-β-lactamase 1 (NDM-1) in the periplasm of live cells.

NDM-1 is one of the main resistance determinants to last resort antibiotics in Gram-negative bacteria[16]. NDM-1 is anchored to the inner leaflet of the outer membrane of Gram-negative bacteria, and it is prone to periplasmic PQC[17]. During an infection, the native immune system response elicits a massive metal depletion at the host-pathogen interface[18,19]. This results in removal of the zinc ions from NDM-1, leading to the accumulation of apoNDM-1, which is destabilized and proteolyzed by two C-terminal periplasmic proteases: Prc and DegP[20]. Thus, this represents an optimal, tunable system to follow PQC in the periplasm using high-resolution in-cell NMR.

[1]Laboratory of Metalloproteins, Institute of Molecular and Cellular Biology of Rosario, National University of Rosario (IBR-CONICET-UNR), Rosario, Argentina. [2]Department of Biophysics, Faculty of Biochemical and Pharmaceutical Sciences (FBIOyF), National University of Rosario (UNR), Rosario, Argentina. [3]Magnetic Resonance Center (CERM) and Department of Chemistry "Ugo Schiff", University of Florence, Sesto Fiorentino, Italy. [4]Cellular-Structural Biology Laboratory, Institute of Molecular and Cellular Biology of Rosario, National University of Rosario (IBR-CONICET-UNR), Rosario, Argentina. [5]Argentinian Platform of Structural Biology and Metabolomics (PLABEM), Rosario, Argentina. ✉e-mail: lgonzalez@ibr-conicet.gov.ar; roberta.pierattelli@unifi.it; binolfi@ibr-conicet.gov.ar; vila@ibr-conicet.gov.ar

https://doi.org/10.1038/s41467-025-62340-6

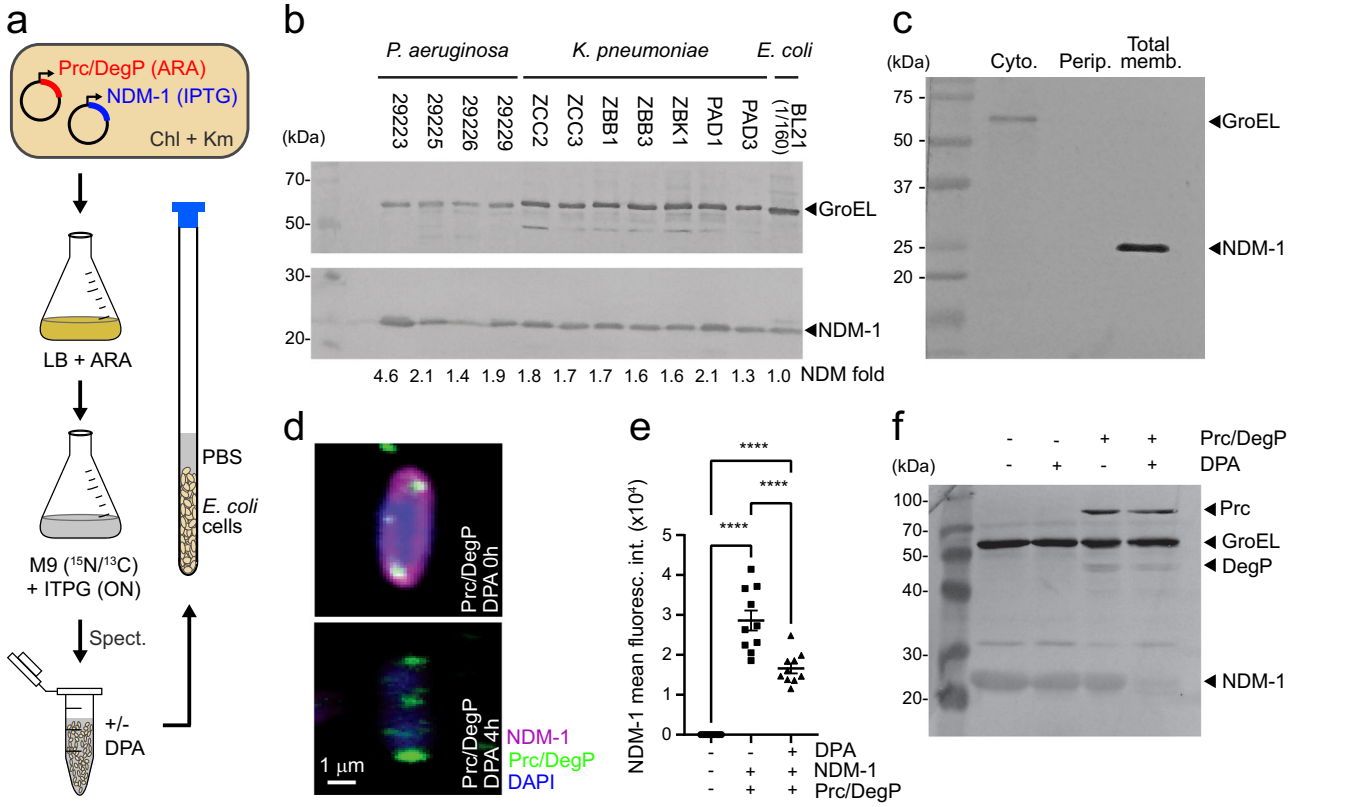



**Fig. 1 | Degradation of apoNDM-1 in the periplasm of live bacterial cells.** **a** Schematic representation of the protocol used for preparing bacterial samples overexpressing NDM-1 and the proteases Prc and DegP. Induction with arabinose (ARA) or IPTG was done at 37 °C and 16 °C, respectively. Incubation with spectinomycin (Spect.) was done at 20 °C. **b** Comparison of NDM-1 overexpression levels from the in-cell NMR samples with *P. aeruginosa* and *K. pneumoniae* clinical strains ($N = 1$). The dilution factor used (1/160) was determined by semi-quantitative western blot analysis and comparisons with the clinical strain *Enterobacter cloacae* 17464 (Supplementary Fig. 1b, c). Normalization was done considering the total number of cells estimated by $OD_{600}$. **c** Membrane localization of overexpressed NDM-1 determined by Western blot analysis. Cyto., Perip., and Total memb. corresponds to cytosolic, periplasmic and total membrane fractions, respectively ($N = 3$). **d** Representative immunofluorescence of NDM-1 (magenta) and Prc and DegP (green) in *E. coli* cells ($N = 3$). **e** Mean fluorescence intensity of NDM-1 in *E. coli* cells. Panel shows a representative analysis of three independent repetitions ($N = 3$). No NDM/DPA = 0.0011 ± 0.0001, NDM/No DPA = 2.8600 ± 0.2494, NDM/DPA = 1.6590 ± 0.1227 (mean ± SEM, $n = 10$ per treatment). Significant difference between conditions, $^{****}p < 0.0001$, Tukey, one-way ANOVA. **f** Western blot analysis of periplasmic NDM-1 degradation by Prc and DegP upon metal deprivation ($N = 3$).

Here we disclose a two-step, sequential degradation process where Prc targets NDM-1 at the membrane, and DegP further degrades the released products. Recognition and cleavage events by Prc depend on both NDM-1 primary sequence and secondary structure content. This work opens perspectives for the mechanistic study of periplasmic processes at atomistic level in live cells.

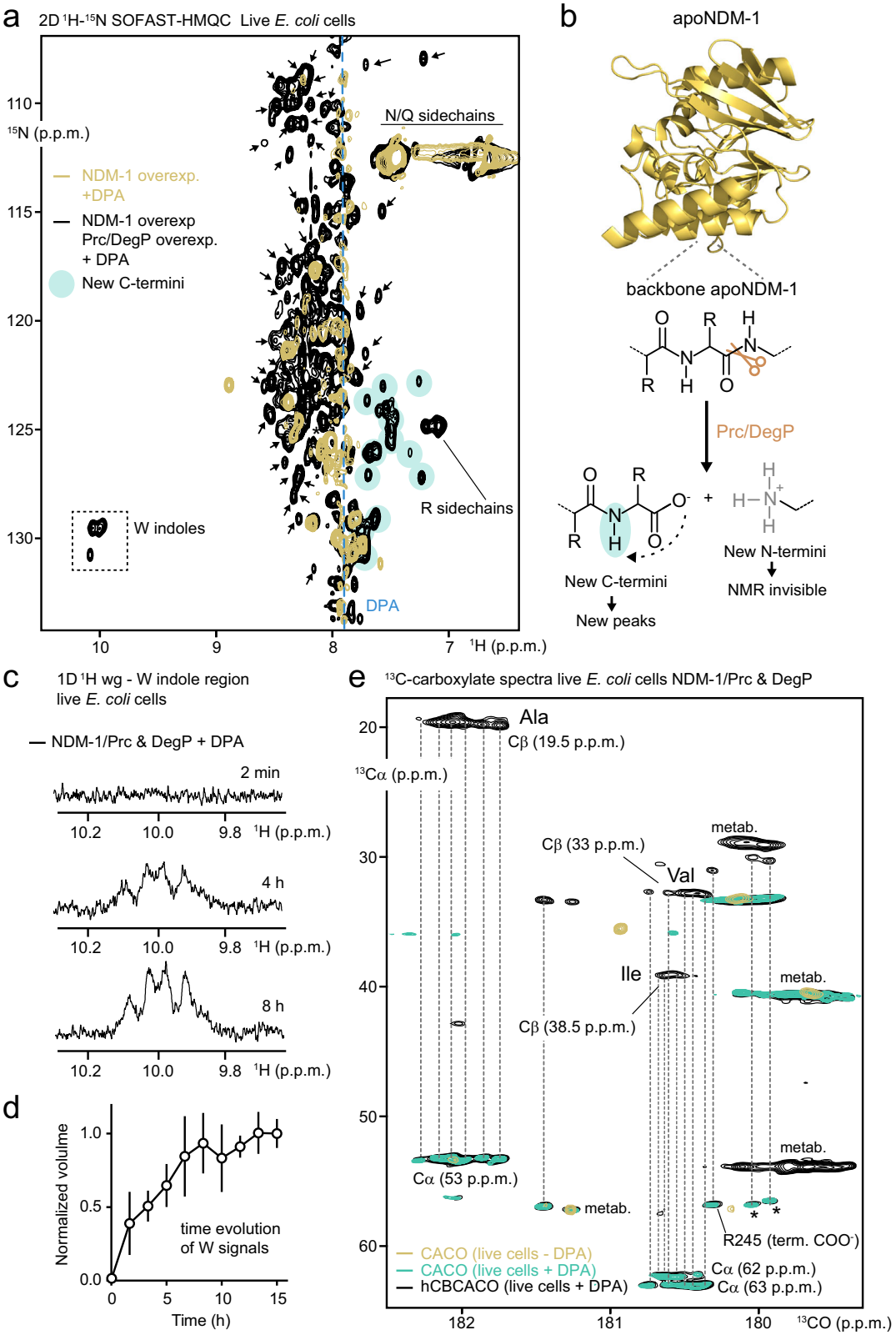
## Results

### Periplasmic NDM-1 degradation generates discrete peptide fragments

The study of the degradation of NDM-1 by in-cell NMR presents several challenges due to the small volume of the periplasm[9] and the requirement to direct the overexpression of NDM-1 to the outer membrane[17], and Prc and/or DegP to the periplasmic space[21,22]. Furthermore, protein levels should be carefully controlled to avoid collateral toxic cellular reactions. Membrane-bound NDM-1 is not expected to give rise to NMR signals due to its slow tumbling rates, while the soluble peptide fragments resulting from its degradation may be detectable by NMR. A dual plasmid system enabling independent induction of labeled membrane-anchored NDM-1 and the unlabeled proteases Prc and/or DegP in *Escherichia coli (E. coli)* was designed to adjust the protease levels according to the NDM-1 concentration (Fig. 1a)[10]. Expression levels of NDM-1 in the periplasm resulted in an average of 190 µM (~19,200 copies of NDM-1) per bacterial cell. These protein levels are at the lower limit of typical in-cell NMR studies[15,23] and are below the number of other abundant periplasmic proteins located in the outer membrane, such as the outer membrane porins (Omp) OmpA (~$10^5$ copies per cell), OmpC (~$10^4$ copies per cell) or OmpF (~$10^4$ copies per cell)[8]. When comparing with a panel of 11 representative clinical isolates (4 *Pseudomonas aeruginosa* (*P. aeruginosa)* and 7 *Klebsiella pneumoniae* (*K. pneumoniae),* (Fig. 1b and Supplementary Fig. 1a–c), the current system presents a 35-fold increase in NDM levels. Importantly, this expression was achieved without perturbing its localization in the outer bacterial membrane (Fig. 1c). Immunofluorescence confocal microscopy confirmed periplasmic co-localization of NDM-1 and Prc/DegP, and NDM-1 degradation in the presence of the chelator dipicolinic acid (DPA), that mimics the natural zinc starvation process[20] (Fig. 1d, e and Supplementary Fig. 2a–d). NDM-1 was distributed homogenously along the bacterial membrane, while the proteases exhibited preferential localization spots in the periplasm. We optimized the expression of DegP and Prc in the presence of DPA, leading to apoNDM-1 degradation (Fig. 1f).

Overexpression of $^{15}$N-labeled NDM-1 maintaining the endogenous protease levels or in the absence of DPA gave rise to NMR signals corresponding to *E. coli* metabolites (Fig. 2a and Supplementary Fig. 3)[24]. Instead, the increase of unlabeled Prc and DegP levels in the presence of DPA revealed a series of new resonances (Fig. 2a) that can be attributed to: (1) NH amide groups with a low dispersion range (7.5–8.5 ppm for $^1$H nuclei), consistent with intrinsically disordered

https://doi.org/10.1038/s41467-025-62340-6




protein/peptide species, (2) tryptophan indole groups and (3) NH amide groups in a typical range of C-terminal residues (Fig. 2a, b and Supplementary Fig. 3)[25]. Real-time NMR experiments showed that the peptide signals from apoNDM-1 build up with time reaching a plateau at ca. 6.5 h (Fig. 2c, d and Supplementary Fig. 4a, b). Protein degradation involves the conversion of carbonyl groups to carboxylates at the targeted residues (Fig. 2b)[25] and can be directly assessed by the $^{13}C$ chemical shifts of these moieties[26,27]. $^{13}C$-based CBCACO and CACO experiments showed a set of resonances with $^{13}CO$ shifts consistent with carboxylate moieties (>180 ppm) present only upon addition of DPA (Fig. 2e and Supplementary Fig. 4c). The identity of these C-terminal residues can be ascertained based on their $^{13}C\alpha$ and $^{13}C\beta$ chemical shifts[28]. Based on this, we established that the C-termini of newly generated peptides correspond to Ala, Val, Ile, and Thr residues,

**Fig. 2 | NMR features of NDM-1 degradation in *E coli*.** **a** 2D $^{1}H$-$^{15}N$ SOFAST HMQC spectra of apoNDM-1 in *E. coli* cells when Prc and DegP were overexpressed (black) and at endogenous protease levels (light brown). Cyan circles identify NMR resonances with chemical shift displacements characteristic of newly generated C-terminal sites. Black arrows denote cross-peaks from amide groups of disordered peptides. The dotted square indicates tryptophan HN indole signals from newly generated apoNDM-1 peptide fragments. The vertical cyan line indicates the artifactual set of signals (T1 noise) caused by the sharp and intense resonance of unlabeled DPA. **b** Schematic representation of the resulting chemical groups upon amide peptide bond cleavage. **c**, **d** Representative time course of periplasmic apoNDM-1 degradation followed by 1D $^{1}H$ NMR analysis of tryptophan HN indole signals (**c**). Experiment was performed on two independent bacterial samples. Tryptophan HN indole NMR signal amplitude plateaus at c.a. 6.5 h (**d**). Each value corresponds to the normalized intensity at each timepoint. Error bars represent the experimental noise in each spectrum. **e** $^{13}C$ detected CBCACO (black) and CACO (cyan) NMR spectra of *E. coli* cells overexpressing NDM-1 and Prc/DegP after DPA treatment or in its absence (yellow). $^{13}CO$ NMR signals above 180 ppm belong to newly generated C-terminal backbone carboxylates. Cα and Cβ chemical shifts in the second spectral dimension identify the type of amino acid side chain. (*) indicate unassigned minor sites. In all cases, NMR spectra were registered at 20 °C.

indicating that Prc and DegP recognize non-charged amino acid side chains in the periplasm of live cells.

The spectral pattern of the supernatant closely resembled that of whole cells and remnants cells (Supplementary Fig. 5a, b). The peptide fraction released to the medium mirrored the set of peptides in the periplasm. Diffusion NMR experiments revealed that these peptides are mostly between 6 and 16 residues long (Supplementary Fig. 5c). We verified that cells remained viable and the integrity of the outer membrane was preserved during NMR acquisitions (Supplementary Fig. 6a, b), suggesting that the extracellular pattern is due to passive peptide release by bacterial secretion systems and/or non-selective porins. Stabilization of LPS by adding $Ca^{2+}$ and $Mg^{2+}$ [29] immediately after DPA treatment resulted in similar spectra, indicating that peptide release is also independent of an extracellular metal restriction response (Supplementary Fig. 6c, d). These observations were reproducible in replicate experiments (Supplementary Fig. 7a, b). Thus, the extracellular NMR peptide pattern provides a bona fide picture of the periplasmic profile, but with higher resolution and stability. We therefore pursued signal assignment and identification of the released fragments in these samples.

## Prc and DegP recognize specific amino acid side chains in vivo

Triple resonance NMR experiments on the supernatants of doubly labeled samples (Supplementary Fig. 8a–e) enabled the identification of 33 resonances corresponding to new C-termini (Fig. 3a–c) generated by the concerted action of Prc and DegP. These corresponded to 18 Ala, 8 Val, 4 Ile, and 3 Thr residues. Their sequential assignment allowed us to pinpoint 23 cleavage sites in the NDM-1 sequence (Supplementary Fig. 9a). We validated this assignment by selectively labeling Lys and Met residues (Supplementary Fig. 9a–c)[30,31]. We did not detect any signals from the first 20 amino acid residues of the protein. Indeed, the signal corresponding to Met14 was the only one absent in the NMR spectra of $^{15}N$-L-Met labeled samples. These results suggest that the proteases degrade the membrane-bound protein from the C-terminus to the first 20 residues, where the lipid moiety is attached, consistent with the known C-terminal protease activity of Prc and DegP. Cell fractionation experiments after DPA treatment confirmed that the degradation process takes place in the membrane (Supplementary Fig. 9d, e).

To assess the specific recognition sites of Prc and DegP, we evaluated their individual activity by expressing each protease gene individually in *E. coli* cells where the other gene was knocked out (Fig. 3d, e and Supplementary Fig. 10). Degradation by Prc-only (Δ*degP* cells) revealed 20 signals corresponding only to Ala (15) and Val (5) C-terminal residues. Instead, in Δ*prc* cells, DegP produced NDM-1 peptides with C-termini corresponding to Ala (11), Val (6), Ile (4), and Thr (2) side chains. These results indicate a higher residue-specificity of Prc compared to DegP. Immunofluorescence experiments showed that the individual proteases localize in the periplasm (Fig. 3f). The processing rate of NDM-1 in live cells was similar in the presence of both proteases and only Prc, while degradation by DegP alone was slower (Fig. 3f, g). These substrate preferences were confirmed at 37 °C using confocal microscopy and NMR (Supplementary Fig. 11). Furthermore, overexpression of Prc maintaining endogenous levels of DegP showed an NMR fragment pattern similar to that observed upon overexpression of both proteases (Supplementary Fig. 10b). In contrast, degradation of apoNDM-1 in cells overexpressing DegP with endogenous Prc levels showed fewer C-terminal signals and with a different cleavage pattern. In vitro digestion of apoNDM-1 by recombinant Prc and DegP reproduced the amino acid specificity observed in live cells. However, the number of targeted sites was lower compared to in vivo (Fig. 3e, Supplementary Fig. 10c and 12a, c). Prc was also able to cleave apoNDM-1 more efficiently than DegP, even at higher DegP concentrations (Supplementary Fig. 12b, d). Mass spectrometry data confirmed the site preferences for each protease (Supplementary Fig. 13a). The smallest peptide detected had 7 amino acid residues (Supplementary Data Files 1–3), in agreement with NMR diffusion data (Supplementary Fig. 5c). MS revealed more processing sites compared to NMR data. The sensitivity of NMR is expected to provide a picture of the abundant peptide fragments, i.e., disclosing the more prevalent cleavage sites (Supplementary Fig. 13b, c).

## Prc and DegP process apoNDM-1 concertedly

Comparison of the NMR spectra of the peptides produced by Prc and DegP or the individual proteases in vivo evidenced different chemical shifts for a restricted set of C-terminal resonances. This was clear for Ala110, Ala116, Ala238, and other unassigned cross-peaks (Fig. 3d, blue arrows). We repeated these experiments in the presence of a protease inhibitor cocktail (PI). Despite being a Ser protease, Prc is not inhibited by these compounds while DegP is[20]. Addition of PI to bacterial cells overexpressing Prc in a *ΔdegP* background did not change the NMR pattern of released peptides while in bacteria expressing DegP (*Δprc* background) degradation was fully inhibited (Supplementary Fig. 13d, e). These observations discard the activity of a third protease processing NDM-1 and thus, are compatible with a mechanism in which DegP processes the products of Prc, changing the proximal chemical environment of the C-termini, resulting in chemical shift displacements. To test this hypothesis, we incubated apoNDM-1 with Prc, DegP and Prc/DegP in vitro and evaluated the degradation process. SDS-PAGE analysis showed the presence of low-MW NDM-1 fragments and small peptide products in the presence of Prc alone that disappeared upon addition of DegP (Fig. 4a, b, and Supplementary Fig. 14a–d). Instead, these fragments were not detected when apoNDM-1 was incubated with DegP alone under crowding conditions that stimulate its protease activity[20]. Even in these conditions, DegP has a minor contribution to the degradation rate of apoNDM-1 by Prc (Supplementary Fig. 14d). In vitro digestions of apoNDM-1 with Prc and DegP showed more C-terminal resonances than with Prc alone, and the new C-termini corresponded to Ile and Val residues which are targeted by DegP (Fig. 4c). Diffusion and MS experiments showed that the peptides processed by Prc and DegP had shorter lengths and confirmed the presence of Ile and Thr C-termini generated by DegP (Supplementary Fig. 13a and 14e, f). These results indicate that DegP contributes to the degradation process mainly by processing peptides released by Prc, and not by directly attacking the full-length protein, in agreement with in-cell NMR observations.

https://doi.org/10.1038/s41467-025-62340-6

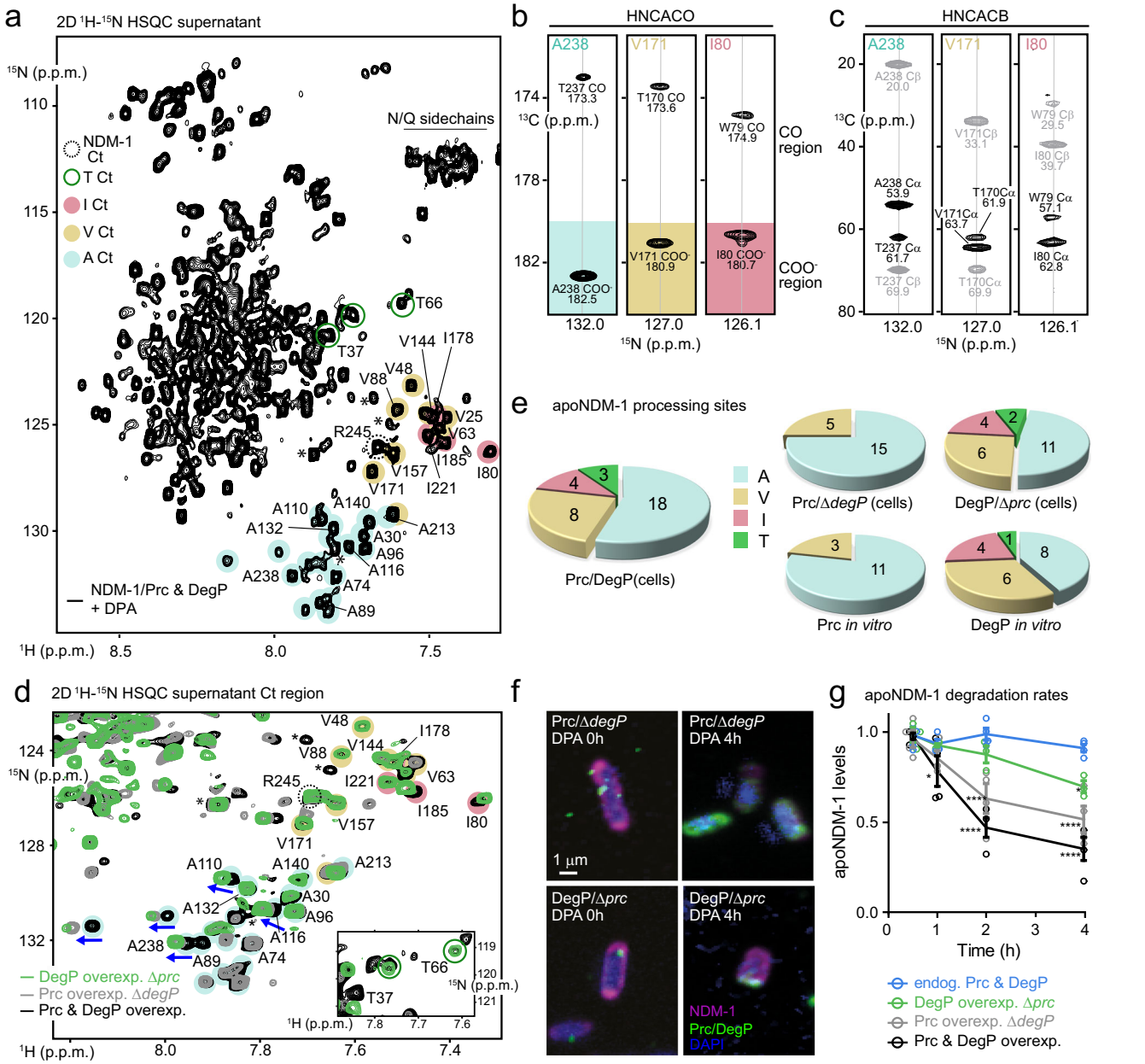



**Fig. 3 | Prc and DegP target apoNDM-1 at specific sites. a** 2D $^{1}$H-$^{15}$N HSQC spectrum of the supernatant of *E. coli* cells overexpressing $^{15}$N/$^{13}$C-isotopically enriched NDM-1 and non-enriched Prc/DegP after DPA exposure and incubation for 4 h at 20 °C. Colored circles denote the newly generated C-termini and the amino acid type: Cyan (alanine), light brown (valine), burgundy (isoleucine) and green (threonine). The assignment of newly generated C-termini and amino acid type was determined by chemical shifts analysis of CO, Cα and Cβ of the corresponding resonance (**b**, **c**). **d** 2D $^{1}$H-$^{15}$N HSQC spectra in the backbone carboxylate region of apoNDM-1 processed by Prc and DegP (black) and by Prc (Δ*degP* background, gray) or DegP (Δ*prc* background, green). Blue arrows indicate NDM-1 NMR signals with chemical shifts displacements when one or both proteases were present. Inset show the spectral region of threonine C-termini. NMR spectra were acquired at 20 °C. **e** Pie chart of apoNDM-1 C-termini generated in the bacterial periplasm by Prc and DegP (left), Prc or DegP (right, first row) and in vitro by Prc or DegP (right, second row). **f** Representative immunofluorescence of NDM-1 (magenta) processing by Prc or DegP (green) in *E. coli* cells ($N = 3$, $n = 10$ per treatment). **g** Analysis of apoNDM-1 degradation by Prc and DegP, Prc or DegP in live *E. coli* cells at 20 °C. ApoNDM-1 levels were measured by Western blot. The data represents mean ± SD. ($N = 4$). Significant difference $^{*}P < 0.05$ and $^{****}P < 0.0001$, Dunnet, two-way ANOVA. Exact, mean ± SD values are enclosed in the source data file.

## Prc targets specific secondary structures

An inspection of the cleavage sites revealed that Prc targets 15 Ala and 5 Val residues, out of a total of 36 and 15, respectively, indicating a strict site preference (Fig. 4d). Cleavage sites were more frequently flanked by residues with small hydrophobic side chains at position −1, and small hydrophobic or uncharged polar side chains at position +1 (Fig. 4e and Supplementary Fig. 14g). However, these characteristics do not fully explain Prc processing preferences, as similar sites remained uncleaved. Mapping the cleavage sites onto the structure of folded holoNDM-1 reveals that most of them are located within β-strands or in neighboring loops. The cleavage sites located in α-helices correspond to: (i) the C-terminal α4 and α5, that become unstructured upon removal of the zinc ions[20] and (ii) α1, which is not expected to maintain the native structure when 70% of the protein has already been proteolyzed. We conclude that Prc avoids cleavage within α-helices. To support this hypothesis, we modeled the interaction between Prc and different degradation products using Alpha-fold 2.0[32]. These models revealed that substrate binding requires pairing of a C-terminal

https://doi.org/10.1038/s41467-025-62340-6

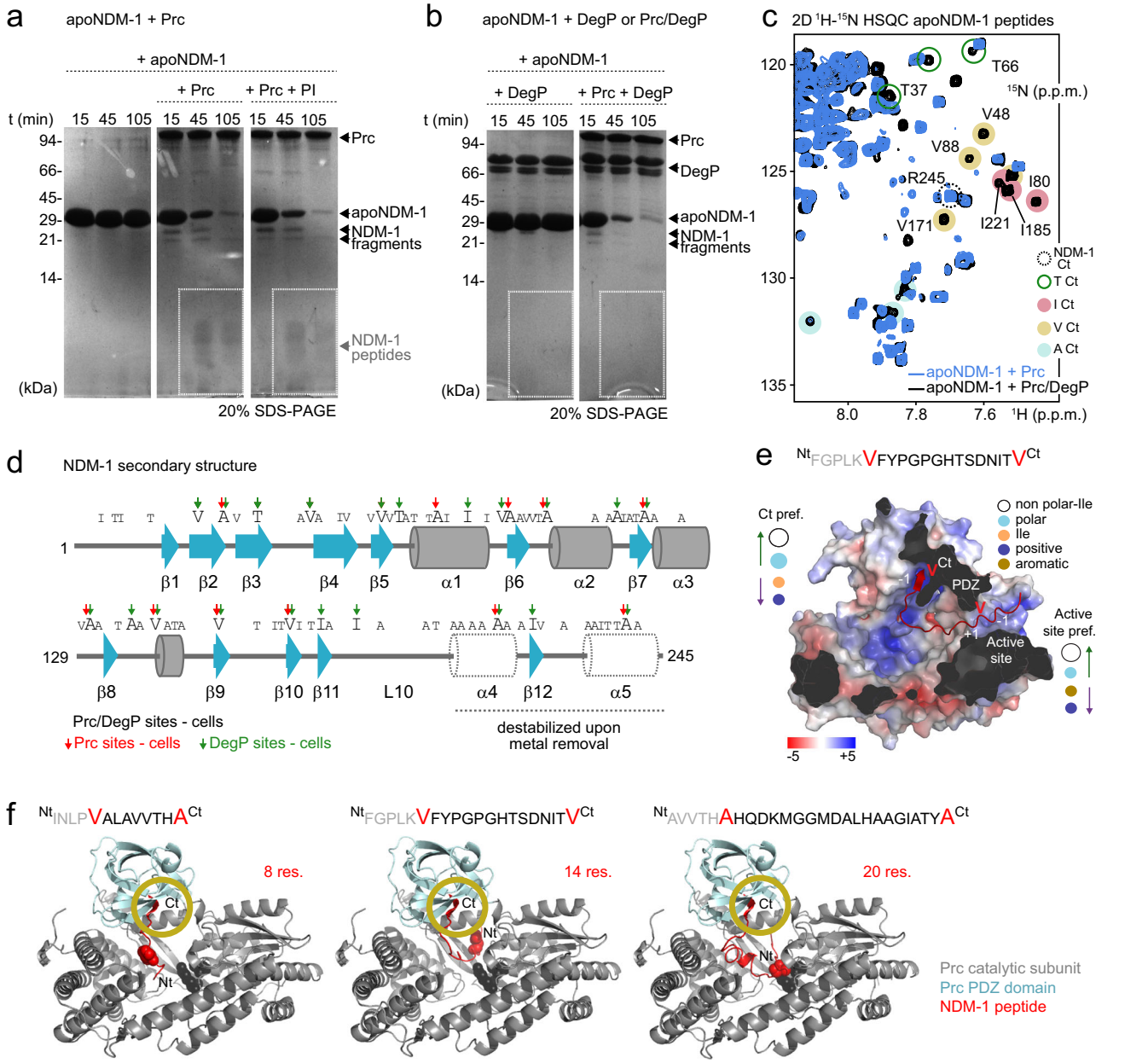



**Fig. 4 | Structural determinants of apoNDM-1 recognition and proteolysis by Prc and DegP.** SDS-PAGE analysis of apoNDM-1 degradation in vitro at 37 °C by Prc (**a**), DegP, or by the concerted action of both proteases (**b**). White dotted squares highlight the presence of low molecular weight peptides produced by Prc activity that are absent when both Prc and DegP are added together to the reaction mixture. PI indicates that a complete protease inhibitor cocktail was added to confirm that Prc is not inhibited. Similar results were obtained in three independent experiments. **c** Overlay of 2D $^{1}$H-$^{15}$N HSQC spectra of peptides resulting from the degradation of apoNDM-1 with recombinant Prc (blue) or Prc/DegP (black). Degradation reactions were done at 37 °C for 4 h. C-terminal signals that are absent when DegP is not added to the reaction mixture are indicated. **d** Mapping of Prc (red arrows) and DegP (green arrows) cleavage sites on apoNDM-1 secondary structure. Both proteases recognize sites in the proximity of β-sheet secondary structure elements. **e** AlphaFold-2 modeling of Prc bound to the apoNDM-1 generated peptide $^{Nt}$FGPLKVFYPGPGHTSDNITV$^{Ct}$ in electrostatic surface. Color circles show the +1 and -1 amino acid side chains preference of Prc for processing apoNDM-1 alanine and valine residues. **f** AlphaFold-2 modeling of Prc bound to apoNDM-1 generated peptides of different length in cartoon mode. Yellow circles highlight the β-pairing (β-augmentation) between the peptide substrate and the PDZ domain of Prc. The C- and N-terminal sites of the peptides are indicated with Ct and Nt, respectively. We included more amino acid residues towards the N-terminus to show the continuation of the protein backbone.

β-strand with another β-strand from the substrate recognition domain (PDZ) of Prc, to properly orient the following cutting site into the catalytic pocket (Fig. 4f, Supplementary Fig. 15). Overall, these results indicate that substrate selection by Prc is driven by the primary sequence and a minimal peptide length in regions prone to adopt β-sheet structures. Furthermore, sequence-context analysis of Ala and Val residues in uncleaved regions outside α-helices suggests that Prc cannot accommodate bulky residues (either aromatic or positively charged) at the narrow substrate funnel entrance (position +1, Fig. 4e and Supplementary Fig. 14g). Ile or positively charged residues were also avoided in position −1, indicating size restrictions and/or charge repulsions in the PDZ domain, which is positively charged to accommodate substrate C-terminal carboxylates[33].

## Discussion

We used in-cell NMR to map the degradation process of apoNDM-1 from the C- to the N- terminus by Prc in the periplasmic side of the outer membrane (Fig. 5). We also identified the individual cleavage

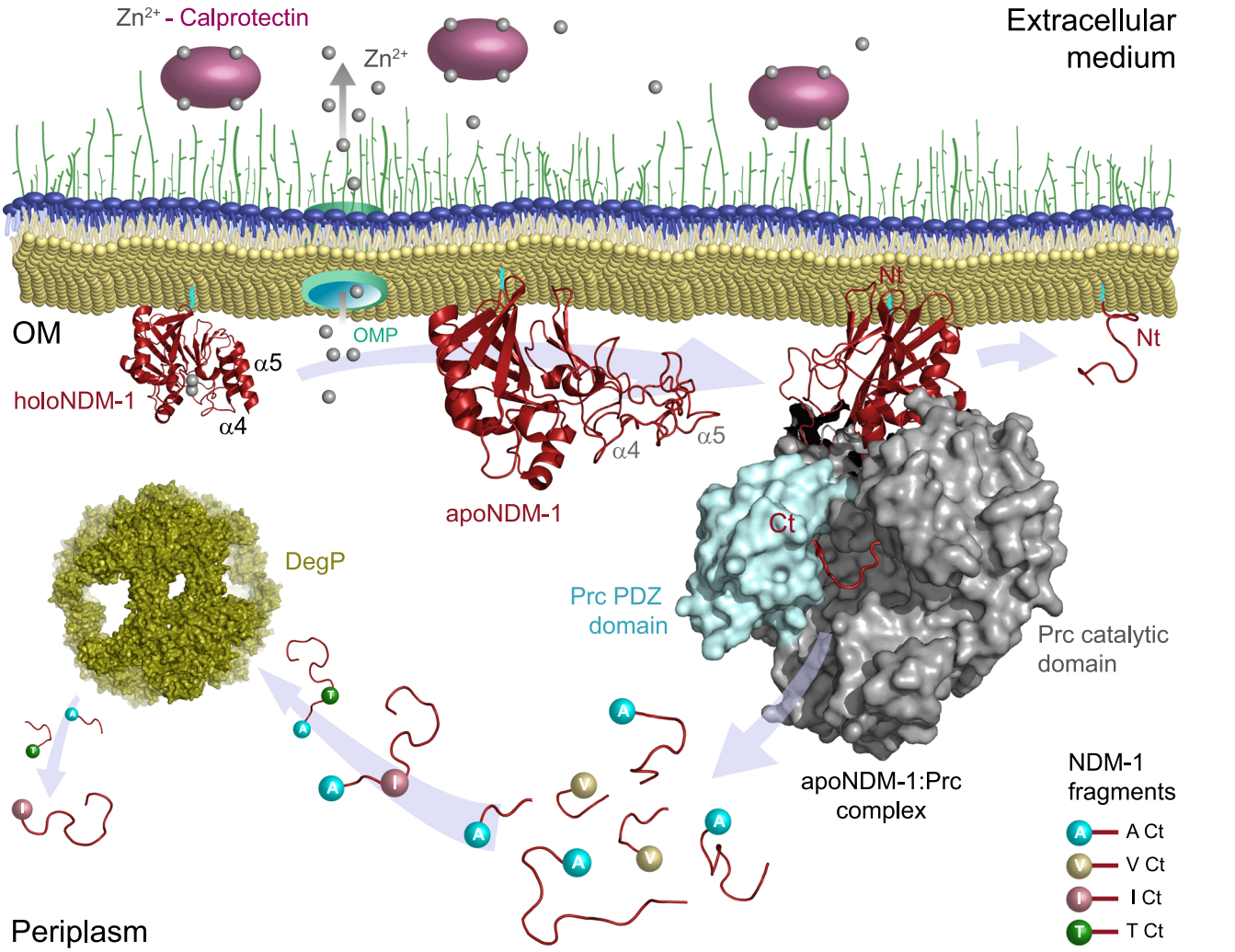



**Fig. 5 | ApoNDM-1 degradation catalyzed Prc and DegP.** Schematic representation of the molecular events elicited by Zn(II) deprivation and destabilization of NDM-1 at the inner leaflet of the bacterial outer membrane (OM). Metal removal results in the loss of α4 and α5 stable helical structure and recognition by Prc at the membrane surface. Prc cleaves apoNDM-1 at specific alanine and valine residues producing peptide fragments that are further process by DegP. Structures were generated with the PDB entries 4EXY (NDM-1), 5WQL (Prc), and 3CS0 (DegP).

sites of the proteases Prc and DegP in live bacteria, with Prc displaying a higher specificity. The pioneering work by Sauer identified the substrate sites of this protease at small, uncharged residues, such as Ala, Cys, Ser, Thr, and Val[34–37]. Here we show that, in vivo, Prc releases peptide fragments with C-terminal Ala and Val residues at defined positions in the protein structure. We also disclose a concerted, sequential mechanism in which Prc products are substrates of DegP. Since the N-terminal sequence remains membrane-bound, we conclude that this process occurs in close proximity to the outer membrane. Interestingly, most Prc substrates are associated with the bacterial membrane, either through direct anchoring or by translocation by effector proteins such as NlpI[22,38–40]. Considering that Prc targets membrane-anchored NDM-1 after metal removal and structural destabilization, we propose that Prc serves as an effective quality control protease for membrane proteins.

Recognition by Prc is not limited to cleavage at non-polar sites, since it avoids proteolysis when the Ala and Val residues are located in structured α-helices. Indeed, cleavage sites are located in β-strands or nearby loops. Prc contains a PDZ domain for substrate recognition. Serendipitous binding of small peptides to PDZ folds in crystal structures have revealed the formation of β-strands of these peptides within the PDZ domain[39]. The herein reported recognition pattern of Prc reveals that client recognition by the PDZ domain requires protein stretches with β-strand propensity. Indeed, the C-terminus in Zn(II)-loaded NDM-1 is a structured α-helix that cannot be recognized and cleaved by Prc unless it becomes unstructured, as it occurs upon zinc limitation[20].

The crystal structure of Prc in the resting state has shown that the PDZ domain acts as a lid that regulates the activity of the protease by reorienting the active site residues upon opening[38,39]. The current DOSY and MS experiments show that Prc requires a minimum distance of 6–8 residues between two consecutive cleavage sites. We speculate that, upon binding to a C-terminus, the PDZ domain pulls the substrate out by at least 6–8 residues to rearrange the active site into a productive conformation. Since the distance between the PDZ domain and the active site in the active form of Prc is 30 Å (the length of an unstructured peptide of 9–10 residues), we propose that this active site reorientation occurs before complete opening of the lid.

These cleavage site preferences allow to explain the degradation of other Prc substrates. Prc processes the penicillin binding protein FtsI by cleaving 11 residues at the C-terminus releasing the mature protein[41]. Inspection of the structure of full length FtsI shows that this stretch is unstructured, while the C-terminus generated after cleavage is residue Val577, located in a α-helical region[42]. We conclude that the Val residue at a α-helix is a stop signal for the protease. By contrast, Prc substrates rich in β-sheet secondary structure at the C-terminus are

efficiently processed[34,40], such as the murein hydrolase MepS, essential for peptidoglycan expansion, whose activity is regulated by Prc-mediated proteolysis[22,40]. Thus, we propose that the proteolysis mechanism of Prc involves the formation of a β-sheet pairing between the substrate and the PDZ domain together with the recognition of Ala and Val residues at the catalytic site. Modeling of NDM-1 peptides bound to Prc indicates that the bowl-shaped structure of Prc is able to accommodate protein fragments of different lengths, supporting a general mechanism of broad substrate selection and cleavage by Prc.

This work shows that in-cell NMR is able to provide atomic details of cellular processes in the restricted subcellular space of the bacterial periplasm and reveals the relevance of monitoring these events in live cells. Moreover, our work shows that NDM-1 peptides generated in the periplasm can be translocated to the extracellular media without a significant compromise of the outer membrane. This implies that whether the detected peptides are within live cells or excreted to the extracellular medium, the processing of NDM-1 occurred in the native environment of the bacterial periplasm. ApoNDM-1 degradation in cells and in reconstituted in vitro reactions were different, both on the positional selection of cleavage sites and the higher catalytic efficiency of the enzyme in the bacterial periplasm. Also, the finding of specific proteolytic hotspots reveals that the periplasm is far from being a homogenous solution, prompting for this type of approach. This paves the way for investigating PQC or other tightly regulated metabolic pathways that are crucial for bacterial pathogenesis and virulence in the periplasm of Gram-negative bacteria, offering clues for the development of antimicrobial therapeutic approaches.

## Methods

### Bacterial strains and reagents

*Escherichia coli* BL21 (DE3) was used for overexpression of NDM-1, DegP and/or Prc knock-out strain constructions, cell fractionation, microscopy and all NMR experiments. *E. coli* DH5α was used for plasmid maintenance. Clinical strains producing NDM-1 *Enterobacter cloacae* 17464[17]; *P. aeruginosa* 29223, 29225, 29226, and 29229; *K. pneumoniae* ZCC2, ZCC3, ZBB1, ZBB3, ZBK1, PAD1, and PAD3, used for protein level comparison, were kindly provided by Fernando Pasteran (ANLIS "Dr. C. G. Malbran", Argentina). Strains were grown aerobically at 37 °C in Luria–Bertani (LB broth) or in M9 minimal media supplemented with kanamycin 50 μg $ml^{-1}$ and/or chloramphenicol 35 μg $ml^{-1}$ when required. Chemical reagents were obtained from Sigma-Aldrich, molecular biology enzymes from Promega, and primers from Life Technologies, except when indicated differently. Complete, EDTA-free protease inhibitor cocktail was from Roche. NMR buffer composition is 20 mM phosphate, 150 mM NaCl at pH 7.0.

### Molecular biology and strain construction

Standard molecular biology techniques were performed according to Sambrook et al.[43]. Primers used in this work were:

prc Fw-p1 gcagaacacctggtgttctgaaacggaggccgggccaggcgtgtaggct ggagctgcttcg; prc Rv-p2 tgttaaaaaatcaggcacaatttcttgtgcctgattgatacat atgaatatcctcctta; Check-prc aacgcaagccacgtccgactac; degP Fw-p1 aca gcaattttgcgttatctgttaatcgagactgaaatacgtgtaggctggagctgcttcg; degP Rv-p2 ggagaaccccttcccgttttcaggaaggggttgagggagacatatgaatatcctcctt a; Check-degP cgcttattccacaaactctcgacgc and Rev P1 cgaagcagctcca gcctacac.

Plasmids: pET26-NDM-1, overexpression of full length wild type NDM-1[17]; pBAD33-Prc, expression of full length Prc with a C-terminal Strep-tag sequence[20]; pBAD33-DegP, expression of full length DegP with a C-terminal Strep-tag sequence[20]; pBAD33-Prc+DegP, Expression of full length Prc and DegP both with a C-terminal Strep-tag sequence[20]; pET28a-Prc and pET28a-DegP, overexpression of mature Prc and DegP without the signal peptide sequence[20]; pKD46 lambda Red-mediated recombinase system[44]; pCP20, lambda Red-mediated recombinase system[44]; pKD3, lambda Red-mediated recombinase system[44].

Strains: *E. coli* BL21(DE3) Δ*degP*, strain for protein overexpression knock-out in *degP* gene (this work); *E. coli* BL21(DE3) Δ*prc*, strain for protein overexpression knock-out in *prc* gene (this work).

Knock-out strains of *E. coli* BL21 (DE3) in periplasmic protease genes *prc* or *degP* were obtained using the Lambda Red-mediated recombinase system, coded in the pKD46 plasmid, as previously described[44]. Briefly, we used the pKD3 plasmid (for $Cm^R$ insertion) and primer pairs *prc Fw*-p1/*prc Rv*-p2 and *degP Fw*-p1/*degP Rv*-p2; Rev P1; Check primers were used for strain verification. Mutant strains were cured from $Cm^R$ cassette afterwards, with the pCP20 plasmid[44].

### Protein immunodetection

Levels of C-terminal tagged proteases were determined by SDS-PAGE followed by Western blot with mouse anti-Strep-Tag® II monoclonal antibodies (Novagen Millipore 71590-3 at 1:1000 dilution). Detection of NDM-1 was performed by using rabbit anti-NDM-1 polyclonal antibodies (ISAL, UNL, Argentina, at 1:2500 dilution). Goat anti-mouse (Calbiochem, DC05L) or goat anti-rabbit (Invitrogen, T2191) immunoglobulin G-alkaline phosphatase conjugates (at 1:5000 dilution) were used as secondary antibodies. Bands were detected by reaction with 5-bromo-4-chloro-3-indolyl phosphate (BCIP)/nitro blue tetrazolium (NBT). PVDF membranes (Thermo Scientific, 88518) were imaged and protein bands were quantified with the ImageJ software[45] and converted to relative protein amounts through a calibration curve. This was done by blotting dilutions of pure NDM-1 standards under the same experimental conditions when necessary. Immunodetection of periplasmic maltose binding protein (MBP, Rockland Immunochemicals, 200-401-385) or cytoplasmic GroEL[45] were performed as leakage or loading controls for periplasmic extracts or spheroplasts and whole cells, respectively. Antisera against GroEL was kindly provided by Dr. Alejandro Viale (generated in rabbits according to conventional procedures) and used at a 1:120,000 dilution. The PageRuler Plus Prestained Protein Ladder (Thermo Scientific, 26616) or Precision Plus Protein Standards Kaleidoscope (BioRad, 161–0375) provided molecular weight standards. Western blots with multiple immunodetected proteins were performed sequentially: after each round of primary and secondary antibody incubation and subsequent detection, PVDF membranes were extensively washed, blocked and re-probed[43]. Detection of NDM-1 in clinical strains was done using the same antibodies we used for *E. coli*. Normalization was done considering the total number of cells estimated by $OD_{600}$ as the anti-GroEL antibody has different specificities towards the different bacterial species.

### Preparation of cells and supernatants for NMR measurements

Saturated cultures of *E. coli* cells were prepared in LB medium supplemented with kanamycin and/or chloramphenicol (for selection of pET26 and pBAD33 plasmids, respectively), and used to inoculate (at 1:100 dilution) 150 mL of fresh LB + antibiotics. Cultures were grown with shaking at 37 °C for 2.5 h. Protease overexpression was induced for 3 h by adding L-arabinose to a final concentration of 0.0002–0.0008%.

Afterward, cells were pelleted in sterile bottles by centrifugation (5 min at 2800 x g, 4 °C) and resuspended in 100 mL M9 medium (final O.D. ~3) supplemented with 0.2 mM $CaCl_2$, 5 mM $MgSO_4$, 1 μg/mL biotin, 10 μg/mL thiamine, 100 μM $ZnSO_4$, 4 g/L glucose ($^{12}C$, Sigma or $^{13}C$, CIL, 1396-10), 1.2 g/L $^{15}NH_4Cl$ (Cortecnet, CN80P10) and kanamycin and/or chloramphenicol. For selective Lysine and methionine isotopically enriched NDM-1 samples, M9 medium was prepared with natural abundance $NH_4Cl$, D-glucose and 0.5 mM of $^{15}N/^{13}C$ enriched L-Lys (Cortecnet, CCN1800P01) or $^{15}N/^{13}C$ L-Met methionine (CCN2000P025) as previously reported[30,31].

After 20 min incubation, IPTG was added to a final concentration of 0.5 mM to induce NDM-1 overexpression and left overnight at 16 °C

with shaking. Cultures were then treated for 30 min at 20 °C with spectinomycin at a final concentration of 200 μg/mL, to stop protein synthesis. Finally, 100 mL of cultures were gently centrifuged (1000 × g for 5 min, 4 °C) and pellets washed with 20 mL of cold 100 mM DPA in NMR buffer (only in the case of DPA-treated samples). In some experiments, cells were then washed with NMR buffer previously treated with Chelex 100 (Bio-Rad) to wash the DPA and deplete metal ions. For NMR of living cells, pellets were gently resuspended with 250 μL of NMR buffer supplemented with 10% $D_2O$, and immediately placed into standard 5 mm NMR tubes (Norell Standard SeriesTM) for spectra acquisition. This procedure ensures that NDM-1, DegP and Prc levels do not alter intracellular localization or compromise cell viability, avoiding artifacts related to large protein overexpression levels.

Supernatants samples for NMR experiments were prepared similarly, but cells were resuspended with 400 μL of chelex-treated NMR buffer, incubated for 4 h statically at 20 °C and gently pelleted (15 min at 1800 × *g*, 4 °C). In some experiments cells were incubated at 37 °C or the incubation buffer was supplemented with 1 mM $CaCl_2$ and 10 mM $MgSO_4$, as indicated in the figures or figure captions. Supernatants were removed, supplemented with 10% $D_2O$ and used for spectra acquisition.

### Cellular fractionation

Extraction of periplasmic proteins was performed as previously described[46]. Briefly, 200 mL of *E. coli* suspensions ($3.2 \times 10^9$ cells/mL), prepared as detailed in the previous section, were pelleted and cells washed once with 10 mM Tris, 150 mM NaCl, pH 8.0. Cells were then resuspended in 10 mM Tris, 3 mM EDTA, 0.75 M sucrose to a final concentration of ($7 \times 10^9$ cells/mL). Then, 0.5 mM PMSF and lysozyme (from chicken egg white, Sigma-Aldrich, protein ≥90%) was added to a final concentration of 0.1 mg/mL, and left for 2 min at 4 °C. Afterwards, 2 volumes of 1.5 mM EDTA pH 8.0 solution was slowly added to the cell suspension with gentle agitation at 4 °C for 10 min. Cells were pelleted, obtaining the periplasmic extract in the supernatant. The pelleted spheroplasts were washed in 10 mM Tris, 1 mM EDTA, 0.25 M sucrose, 1 mM PMSF, pH 8.0 and resuspended in the same volume of this buffer. Spheroplast formation was confirmed under the microscope.

Total membranes were prepared from spheroplast suspensions as already described[20]. Briefly, spheroplasts were disrupted by sonication (Branson, 30%, 3 pulses of 10 s, with waiting periods of 30 s) and cell debris were removed by centrifugation at 14,000 × *g* and 4 °C for 20 min. Membranes were pelleted by ultracentrifugation (Beckman Optima L-90K Ultracentrifuge, Ti90 rotor) at 150,000 × *g* and 4 °C for 1 h, washed, ultracentrifuged and resuspended in the same buffer. Quantification was done by determination of the total protein content using the Pierce® BCA Protein Assay Kit.

### Viability and leakage controls

The viability of *E. coli* cells after NMR acquisition was evaluated by counting colony-forming units (CFUs) on LB-agar plates inoculated with 10 μL drops from serial dilutions of the cell suspensions. To investigate potential leakage of periplasmic components during DPA treatment, the presence of the periplasmic MBP protein was analyzed by immunodetection. These analyses were conducted on both DPA-treated and untreated samples, compared with normalized quantities of their respective extracellular media.

### Time-dependence of bacterial NDM-1 levels upon Zn(II) depletion

These experiments were done with *E. coli* cells overexpressing NDM-1 and Prc/DegP, or Prc or DegP individually. *E. coli* suspensions prepared under the same conditions as for NMR acquisitions were divided into two. One portion was washed with 100 mM DPA in NMR buffer and then chelex-treated NMR buffer, while the other was washed with chelex-treated NMR buffer (untreated control). Cell suspensions were incubated at 25 °C for a period of 4 h taking aliquots at different time intervals for SDS-PAGE and immunodetection. Cellular NDM-1 amounts in DPA-treated samples were reported relative to the corresponding values in untreated samples[20].

### Detection of cellular NDM-1 by immunofluorescence microscopy

Images were obtained for *E. coli* cells, overexpressing NDM-1 with Prc and DegP proteases at 0 and 4 h after DPA treatment. Cells were plated in Poly-D-Lysine coated coverslips for 30 min, washed twice with PBS and fixed with 0.5 ml of 4% paraformaldehyde solution in PBS for 10 min. After fixation, cells were permeabilized with 0.1% Triton X-100 solution in PBS for 1 min. Subsequently, cells were incubated with an NDM-1 polyclonal antibody (ISAL, UNL, Argentina, at 1:1000 dilution) and Strep-Tag II monoclonal antibodies (Novagen Millipore 71590-3, 1:100) and detected by incubation with anti-mouse CyTM2 conjugated secondary antibodies (Jackson IR, 115-225-003, 1:1000) and anti-rabbit RRX conjugated secondary antibodies (Jackson IR, 111-295-003, 1:1000). After incubation with the secondary antibodies, we added 1:20000 of 4′,6-diamidino-2-fenilindol (DAPI, Sigma, 5 mg/mL stock) to stain DNA. Cells were mounted with SlowFade Antifade reagent (Molecular Probes) and analyzed in a Zeiss LSM880 confocal microscope (Zeiss, Germany).

### Expression and purification of recombinant proteins

Soluble Prc, DegP and mature NDM-1 (Δ38) were overexpressed in *E. coli* BL21(DE3) and purified according to procedures previously set up in the lab[20]. Briefly, bacterial cultures were grown at 37 °C in M9 minimal medium (NDM-1) supplemented with $^{12}$C-Glucose (4 g/L) and $^{15}NH_4Cl$ (1 g/L), or in LB (proteases) until $OD_{600nm} = 0.6$. Then, protein overexpression was induced by addition of 0.5 mM IPTG and, in the case of NDM-1, 0.5 mM $ZnSO_4$. For NDM-1, induction was done ON at 18 °C. For Prc and DegP, induction was performed for 45 min at 37 °C to avoid autoproteolysis. Cells were lysed by sonication and the insoluble material was removed by centrifugation. Proteins were purified using Ni-Sepharose affinity chromatography, the His-tag was cleaved by treatment with Thrombin (or TEV protease in the case of NDM-1) (Sigma-Aldrich, manufacturer protocol), and the tag was removed by a second chromatographic step with the Ni-Sepharose resin. All liquid chromatpography steps were done using an AKTA FPLC instrument (ÄKTA goTM Cytiva). The purified proteins were concentrated using a 10-kDa MW cut-off Centricon device (Millipore, Bedford, MA, USA). Protein concentrations were determined from the absorbance at 280 nm, using molar absorption coefficients (ε280 nm) calculated from aromatic residues by Expasy ProtParam, available at web.expasy.org/protparam/(NDM-1 Δ38, ε280 nm = 27960 $M^{-1} cm^{-1}$; Prc, ε280 nm = 60280 $M^{-1} cm^{-1}$), or by Pierce® BCA Protein Assay Kit (for DegP).

Apo-NDM-1 was obtained by extensive dialysis with EDTA as previously reported[17]. In brief, two rounds of dialysis of the purified holoprotein (ca. 200 μM) were performed against 100 volumes of 10 mM HEPES, 200 mM NaCl, 20 mM EDTA, pH 7.5 over a 12-h period under stirring. EDTA was then removed by three dialysis steps against 100 volumes of 10 mM HEPES, 1 M NaCl, pH 7.5, Chelex 100, and three dialysis steps against 100 volumes of 10 mM HEPES, 200 mM NaCl, pH 7.5, Chelex 100. For NMR measurements, the protein solution was exchanged to NMR buffer by a final dialysis step. All buffer solutions used to prepare the apo-enzymes were treated by extensive stirring with Chelex 100 (Bio-Rad).

### Proteolysis of recombinant apoNDM-1

Pure recombinant apoNDM-1 (50 μg) was incubated with pure recombinant Prc and/or DegP at 37 °C using a molar ratio of 4:1, in 50 mM HEPES, 200 mM NaCl, pH 7.0 previously treated with Chelex 100, with or without addition of 100 mg/mL Ficoll70. Aliquots were taken at

different times and subjected to SDS-PAGE and Coomassie blue staining.

Solutions of NDM-1 peptides for MS identification or protease activation experiments were prepared by incubating recombinant apoNDM-1 (100 μg) with Prc, DegP, or a combination of Prc and DegP (4:1 NDM-1:protease ratios) at 37 °C until degradation was complete (3 h for Prc or Prc+DegP; 24 h for DegP alone). Samples were passed through a 10-kDa MW cut-off Centricon device, and NDM-1-derived peptides were collected from the flow-through. Peptides were diluted 1:10 in distilled water and analyzed by mass spectrometry. For NMR experiments, peptides were prepared in the same way but we used 100 μM $^{15}$N uniformly enriched apoNDM-1 and non-isotopically enriched Prc or Prc+DegP. The samples were filtered as above and used without further dilutions.

### LC-MS analysis

Peptide separations were carried out on a nanoHPLC Ultimate3000 (Thermo Scientific) using a nano column EASY-Spray ES901 (15 cm × 50 μm ID, PepMap RSLC C18). The mobile phase flow rate was 300 nL/min using 0.1% formic acid in water (solvent A) and 0.1% formic acid and 100% acetonitrile (solvent B). The gradient profile was set as follows: 4–30% solvent B for 10 min, 30–80% solvent B for 2 min and 80% solvent B for 1 min. 2.50 μl of the sample were injected. MS analysis was performed using a Q-Exactive HF mass spectrometer (Thermo Scientific). For ionization, 1.9 kV of liquid junction voltage and 300 °C capillary temperature was used. The full scan method employed a m/z 200–2500 mass selection, an Orbitrap resolution of 120,000 (at m/z 200), a target automatic gain control (AGC) value of 1e6, and maximum injection times of 100 ms. After the survey scan, the five most intense precursor ions were selected for MS/MS fragmentation.

Fragmentation was performed with a normalized collision energy of 27 eV and MS/MS scans were acquired with a dynamic first mass, AGC target was 5e5, resolution of 30,000 (at m/z 200), isolation window of 1.4 m/z units and maximum IT was 55 ms. Charge state screening was enabled to reject unassigned, singly charged, and equal or morethan six protonated ions. A dynamic exclusion time of 10 s was used to discriminate against previously selected ions.

MS data were analyzed with Proteome Discoverer (V: 2.1.4.1.15), using standardized workflows. Mass spectra *.raw files were searched against the database of *E. coli* BL21 DE3 from Uniprot. An open search was carried out to identify peptides of variable length between 4 and 144 amino acids, (Parameter: No-Enzyme Unspecific). Precursor and fragment mass tolerance were set to 10 ppm and 0.02 Da, respectively. Variable modifications: protein N-terminal acetylation and methionine oxidation. The mass spectrometry proteomics data have been deposited to the ProteomeXchange Consortium via the PRIDE[47] partner repository with the dataset identifier PXD065625.

### Alpha fold 2 predictions

The predicted structures of Prc bound to NDM-1 peptide substrates were obtained from the sequence of Prc (*E. coli* K12, Uniprot P23865) and the NDM-1 peptides $^{INLP}$*V*ALAVVTH*A*, $^{FGPLK}$*V*FYPGPGHTSDNIT*V* and $^{AVVTH}$*A*HQDKMGGMDALHAAGIATY*A*. Amino acids in italics denote experimentally identified C-termini, while the short sequences in superscripted were added for continuity towards the N-terminus. Each simulation was done separately by submitting the sequence of Prc and each peptide as separate chains to the AlphaFold2_advanced Colab at https://colab.research.google.com/github/sokrypton/ColabFold/blob/main/beta/AlphaFold2_advanced.ipynb[48] using the default settings. This colab does not use templates. PDB files of the Prc:NDM-1 peptide complexes are available as supplementary data files.

### NMR spectroscopy

All NMR spectra were acquired at 20 °C on samples dissolved or resuspended in NMR buffer supplemented with 10% $D_2O$. We used the following NMR spectrometers: (i) for $^{1}$H/$^{15}$N detected experiments 600 MHz Bruker Avance II with a TXI (5 mm $^{1}$H/D-$^{13}$C/$^{15}$N) probe, 700 MHz Bruker Avance III with a TXI (5 mm $^{1}$H/D-$^{13}$C/$^{15}$N) probe, 950 MHz Bruker Avance Neo with a cryogenically cooled TCI probe (5 mm $^{1}$H/D-$^{13}$C/$^{15}$N); (ii) For $^{13}$C detected experiments 700 MHz Bruker Avance Neo with a cryogenically cooled TXO probe (5 mm $^{13}$C/$^{15}$N-$^{1}$H-D) and 1.2 GHz Bruker Ascend with a cryogenically cooled TXO probe (5 mm $^{13}$C/$^{15}$N-$^{1}$H-D).

### NMR experiments on live bacteria

1D $^{1}$H NMR spectra were acquired using a 950 MHz TCI and 1.2 GHz TXO NMR spectrometers. We used the *zgesgp* pulse sequence for efficient water suppression[49]. NMR parameters were 16 K points, 32 scans, a recycling delay of 1.5 s and a sweep width of 16 ppm (transmitter frequency offset 4.69 ppm). Spectra were processed by qsine multiplication and baseline corrected.

1D $^{15}$N-edited $^{1}$H spectra were acquired on a 700 MHz TXI. We used a T1 optimized version of the HSQC pulse sequence[50] or the SOFAST version of the HMQC[51]. NMR parameters were 2 K points, 512 scans, a recycling delay of 0.25 s, and a sweep width of 16 ppm (offset 4.69 ppm). Spectra were zerofilled to 4 K, processed using a sine bell shifts window function multiplication and baseline correction.

For 2D $^{1}$H-$^{15}$N correlation spectra, we used 700 MHz TXI and 950 MHz TCI spectrometers. We used a T1 optimized version of the HSQC pulse sequence[50] or the SOFAST version of the HMQC pulse sequence[51]. NMR parameters were 1 K and 128 points, in the $^{1}$H and $^{15}$N dimension, respectively. We used 384/128 scans depending on the NMR probe (TXI or TCI), a recycling delay of 0.25 s and sweep widths of 16 and 40 ppm in $^{1}$H and $^{15}$N (offsets 4.69 and 119 ppm). To observe the non-aliased NMR signals of Arg side chains and differentiate them from newly generated C-termini (Supplementary Fig. 3b) we used a sweep width of 104 ppm (offset 90 ppm) in the $^{15}$N dimension. NMR experiments of bacterial samples selectively enriched with $^{15}$N/$^{13}$C L-Met or $^{15}$N/$^{13}$C L-Lys was done using the same parameters with the following modifications: for isotopically enriched L-Met samples we used 1 K and 128 points in $^{1}$H and $^{15}$N dimensions, respectively, for a sweep width of 16 and 40 ppm. (offsets 4.69 and 119 ppm) and 384 scans. For L-Lys samples we used 1 K and 56 points in $^{1}$H and $^{15}$N dimensions, respectively, for a sweep width of 16 and 14.5 ppm (offsets 4.69 and 125 ppm) and 384 scans. These experiments were done with $^{13}$C carbon decoupling. In all cases, spectra were zerofilled to 2 K and 1 K in $^{1}$H and $^{15}$N dimensions, respectively, processed using a sine bell shifts window function multiplication and baseline corrected in both dimensions.

Diffusion experiments (DOSY) were done on a 700 MHz TXI. We used four type of samples: i) live cells overexpressing NDM-1 and the proteases Prc/DegP and treated with DPA; ii) synthetic peptides, peptide 1 (AcMDVFMK-$NH_2$, 0.5 mM, 6 amino acid residues, 0.8 kDa), peptide 2 (Ac-LSMPYRTFRRRRPVHN-$NH_2$, 0.5 mM, 16 amino acid residues, 2.1 kDa); iii) free L-Met amino acid (0.5 mM, 0.15 kDa), and iv) peptide mixtures obtained from the degradation of recombinantly purified apoNDM-1 with Prc or Prc/DegP and a filtration step using an Centricon device (10-kDa MW cut-off) to remove the proteases. Samples were dissolved in NMR buffer supplemented with 10% $D_2O$ and with 0.5 μL of 1,4 dioxane (99.8 % Sigma). We used a pulse sequence with longitudinally encode/decode (LED) bipolar gradient pulses for diffusion and presaturation (44 dB) for water suppression during the relaxation delay (ledbpgppr2s)[52]. For each sample we collected series of 24 1D $^{1}$H spectra at increasing gradient amplitudes linearly. Diffusion time was 0.1 s and the diffusion gradient length was 4.4 μs. We used 8 K points in the direct dimension, a sweep width of 16 ppm (offset at 4.69 ppm), 512 scans and a recycling delay of 1.5 s. Processing was done in the direct dimension using a qsine bell shift window function multiplication and baseline correction. DOSY plots were obtained using the DOSY analysis tool from Topspin 3.5. Intensity decay curves were obtained by integrating signals from the 1D proton spectra between

0.65 and 0.95 ppm (peptide methyl groups) and the dioxane signal at 3.67 ppm using the Topspin 3.5 relaxation tool. In these conditions, the diffusion coefficient of dioxane was ~$1.1 \times 10^{-9}$ $m^2/s$ in agreement with previous NMR determinations[53].

$^{13}C$ detected CACO and CBCACO were acquired on a 700 MHz TXO. Acquisitions were done using pulse sequences with an IPAP block and pulse parameters as previously described[54]. For CACO experiments we collected 1 K and 128 points with a sweep width of 29.9 and 40 ppm for $^{13}CO$ and $^{13}C\alpha$ dimensions, respectively (offsets at 173 and 47 ppm), 32 scans and a recycling delay of 0.8 s. Spectra were zerofilled to 2 K and 1 K for $^{13}CO$ and $^{13}C\alpha$, processing was done using a qsine bell shift window function multiplication, forward linear prediction in quadrature mode (32 coefficients) and baseline correction in both dimensions. Similarly, CBCACO experiments we collected 1 K and 156 points with a sweep width of 29.9 and 59.2 ppm for $^{13}CO$ and $^{13}C\alpha/C\beta$ dimensions, respectively (offsets at 173 and 42.2 ppm), 32 scans and a recycling delay of 0.8 s. Spectra were zerofilled to 2 K and 1 K for $^{13}CO$ and $^{13}C\alpha/C\beta$, processing was done using a qsine bell shift window function multiplication, forward linear prediction in quadrature mode (40 coefficients) and baseline correction in both dimensions.

$^{13}C$ detected $^{BEST}CON$ spectra were acquired on a 1.2 GHz TXO. Acquisition was done with standard pulse parameters, as previously described[55]. We collected 1 K and 128 points with a sweep width of 19.5 and 38 ppm for $^{13}CO$ and $^{15}N$ dimensions, respectively (offsets at 173 and 120 ppm), 32 scans and a recycling delay of 0.8 s. Spectra were zerofilled to 2 K and 1 K for $^{13}CO$ and $^{15}N$, processing was done using a qsine bell shift window function multiplication, forward linear prediction in quadrature mode (40 coefficients) and baseline correction in both dimensions.

### NMR experiments on bacterial supernatants

Spectra were acquired using a 700 MHz TXI and a 950 MHz TCI. We used the fast HSQC pulse sequence from Topsin (*fhsqcf3gpph*)[56]. NMR parameters were 2 K and 128 points, in the $^1H$ and $^{15}N$ dimension, respectively. Parameters were 16 scans, a recycling delay of 1 s and sweep widths of 16 and 40 ppm in $^1H$ and $^{15}N$ (offsets 4.69 and 119 ppm). Spectra were zerofilled to 4 K and 2 K in $^1H$ and $^{15}N$ dimensions, processed using a qsine bell shifts window function multiplication, forward linear predicted in quadrature mode (four coefficients) and baseline corrected in both dimensions.

To assign the NMR signals of NDM-1 peptides we acquired standard triple resonance experiments on the supernatant of bacterial samples. These were: (i) HNCO (*hncogpwg3d*) and HNCACO (*hncacogpwg3d)*, 2 K, 48, and 96 points in the $^1H$, $^{15}N$ and $^{13}CO$ dimensions, respectively, sweep width of 11, 41.2, and 14.4 ppm (offsets 4.69, 117, and 173.5 ppm), 8 scans and a recycle delay of 1 s; (ii) HNCOCACB (*hncocacbgpwg3d*) and HNCACB (*hncacbgpwg3d*) 2 K, 48 and 128 points in the $^1H$, $^{15}N$ and $^{13}C\alpha/C\beta$ dimensions, respectively, sweep width of 11, 41.2, and 80.48 ppm (offsets 4.69, 117, and 43 ppm), 8 scans and a recycle delay of 1 s. Overlay of the 2D $^1H$-$^{15}N$ HSQC spectra before and after the triple resonance NMR acquisitions showed minor differences indicating that no significant degradation occurred while acquiring the 3D experiments (Supplementary Fig. 8b), further supporting our previous observations that cell remained intact during NMR acquisitions and that there was no leakage of active proteases, including overexpressed DegP and Prc, to the extracellular medium.

Backbone and Cβ resonance assignment of apoNDM-1 peptides was done following the standard sequential approach[57]. While this strategy is challenging because there are multiple proteolytic interruptions in the primary sequence and chemical exchange broadening vanishes the first and second resonances of residues from newly generated N-terminal groups[25] the excellent resolution and signal-to-noise ratios of the triple resonance experiments produced by the small, fast-tumbling disordered peptides allowed us to assigned 138 amino acid residues spanning different proteins regions (Supplementary Figs. 8c–e, 9a–c, Supplementary Data File 4 and BMRB 53232). The remaining resonances could not be unambiguously assigned due to low signal-to-noise, severe signal overlap from the peptide fragments or ambiguities in the primary sequence.

To validate our assignment, we repeated the 2D $^1H$-$^{15}N$ HSQC spectra using selective Lys and Met isotopic labeling. Using these types of samples, only Lys and Met signals are visible in the NMR spectra, providing confirmation of resonances that belong to those residues. Lys and Met signals in the selective amino acid labeled samples overlapped with the Lys and Met resonances previously assigned on the $^{15}N$-$^{13}C$ uniformly enriched samples (Supplementary Fig. 9a–c).

### Real-time, in vitro NDM-1 degradation

NMR spectra of pure apoNDM-1 (200 µM) were registered in NMR buffer at 25 °C using a 700 MHz TXI spectrometer. Backbone resonance assignment of apoNDM-1 was previously published[20]. We used the $^1H$-$^{15}N$ fast HSQC pulse program (*fhsqcf3gpph*). NMR parameters were: 2 K and 128 points in the $^1H$ and $^{15}N$ dimensions, respectively, a sweep width of 16 and 40 ppm (offsets 4.7 and 119), 12 scans and a recycling delay of 1 s. With this NMR setup the experimental time was 29 min. Next, we repeated this experiment under identical conditions but with the addition of 1 µM Prc or 50 µM DegP and we acquired consecutive $^1H$-$^{15}N$ HSQC spectra to delineate apoNDM-1 degradation kinetics. We had to increase the concentration of DegP to detect a small percentage of apo NDM-1 degradation because the protein is not very active under diluted, non-crowded conditions[20].

### Acquisition, processing, analysis, and illustration of NMR spectra

All spectra were acquired and processed using Topsin versions (3.5, 4.0, and 4.1) (Bruker Biospin). apoNDM-1 indole Trp signals from 1D $^1H$ spectra of live cells were quantified using the standard Topspin integration tool. All indole signals were integrated together and integration limits were selected on proximal local minima. Integral values were plotted as a function of time to obtain the degradation curves using GraphPad Prism. Error bars correspond to the noise integral in each spectrum. 1D $^1H$ and 1D $^{15}N$-edited $^1H$ spectra were exported as csv files using Topspin and plotted on GraphPad Prism. 2D NMR spectra were analyzed using Sparky[58]. Signal intensities for 70 non-overlapped apoNDM-1 cross-peaks (spanning all protein regions) in the presence of Prc or DegP were extracted with Sparky and plotted as a function of time to obtain the degradation curves using GraphPad Prism. 2D NMR spectra were exported as post-script files with Topspin or Sparky and plotted using Adobe Illustrator. Sequential assignment of apoNDM1 peptides was done with CARA (Computer Aided Resonance Assignment, cara.nmr.ch). Strips from the HNCACO and HNCACB were exported as pdf using CARA and plotted using Adobe Illustrator.

### Reporting summary

Further information on research design is available in the Nature Portfolio Reporting Summary linked to this article.

## Data availability

The data supporting the findings of this study are available within the article and supplementary information. The mass spectrometry data generated in this work have been deposited in the ProteomeXchange database under accession code PXD065625. The NMR data generated have been deposited in the Biological Magnetic Resonance Data Bank database under accession code 53232. PDB codes of previously published structures used in this study are 4EXY (NDM-1), 5WQL (Prc) and 3CS0 (DegP). Supplementary Data files contain Supplementary Figs., MS tables and chemical shift assignments of digested NDM-1, assigned $^1H$-$^{15}N$ HSQC of NDM-1 peptides and PDBs of Prc:NDM-1 peptide complexes. Source data are provided with this paper as a Source Data file.

## References


1. Mitchell, A. M. & Silhavy, T. J. Envelope stress responses: balancing damage repair and toxicity. *Nat. Rev. Microbiol.* **17**, 417–428 (2019).
2. Ehrmann, M. *The Periplasm* (American Society for Microbiology Press, 2007).
3. Miller, S. I. & Salama, N. R. The gram-negative bacterial periplasm: size matters. *PLoS Biol.* **16**, e2004935 (2018).
4. Rowley, G., Spector, M., Kormanec, J. & Roberts, M. Pushing the envelope: extracytoplasmic stress responses in bacterial pathogens. *Nat. Rev. Microbiol.* **4**, 383–394 (2006).
5. Merdanovic, M. et al. Protein quality control in the bacterial periplasm. *Annu. Rev. Microbiol.* **65**, 149–168 (2011).
6. Clausen, T., Kaiser, M., Huber, R. & Ehrmann, M. HTRA proteases: regulated proteolysis in protein quality control. *Nat. Rev. Mol. Cell Biol.* **12**, 152–162 (2011).
7. Miot, M. & Betton, J. M. Protein quality control in the bacterial periplasm. *Microb. Cell Fact.* **3**, 4 (2004).
8. Weiner, J. H. & Li, L. Proteome of the *Escherichia coli* envelope and technological challenges in membrane proteome analysis. *Biochim. Biophys. Acta.* **1778**, 1698–1713 (2008).
9. Pilizota, T. & Shaevitz, J. W. Fast, multiphase volume adaptation to hyperosmotic shock by *Escherichia coli*. *PloS one* **7**, e35205 (2012).
10. Burz, D. S., Dutta, K., Cowburn, D. & Shekhtman, A. Mapping structural interactions using in-cell NMR spectroscopy (STINT-NMR). *Nat. Methods* **3**, 91–93 (2006).
11. Li, C. et al. Protein (19)F NMR in *Escherichia coli*. *J. Am. Chem. Soc.* **132**, 321–327 (2010).
12. Luchinat, E., Cremonini, M. & Banci, L. Radio signals from live cells: the coming of age of in-cell solution NMR. *Chem. Rev.* **122**, 9267–9306 (2022).
13. Sakakibara, D. et al. Protein structure determination in living cells by in-cell NMR spectroscopy. *Nature* **458**, 102–105 (2009).
14. Serber, Z. et al. Investigating macromolecules inside cultured and injected cells by in-cell NMR spectroscopy. *Nat. Protoc.* **1**, 2701–2709 (2006).
15. Theillet, F. X. In-cell structural biology by nmr: the benefits of the atomic scale. *Chem. Rev.* **122**, 9497–9570 (2022).
16. Bahr, G., Gonzalez, L. J. & Vila, A. J. Metallo-β-lactamases in the age of multidrug resistance: from structure and mechanism to evolution, dissemination, and inhibitor design. *Chem. Rev.* **121**, 7957–8094 (2021).
17. Gonzalez, L. J. et al. Membrane anchoring stabilizes and favors secretion of New Delhi metallo-β-lactamase. *Nat. Chem. Biol.* **12**, 516–522 (2016).
18. Corbin, B. D. et al. Metal chelation and inhibition of bacterial growth in tissue abscesses. *Science* **319**, 962–965 (2008).
19. Murdoch, C. C. & Skaar, E. P. Nutritional immunity: the battle for nutrient metals at the host-pathogen interface. *Nat. Rev. Microbiol.* **20**, 657–670 (2022).
20. Gonzalez, L. J. et al. In-cell kinetic stability is an essential trait in metallo-β-lactamase evolution. *Nat. Chem. Biol.* **19**, 1116–1126 (2023).
21. Harkness, R. W. et al. Competing stress-dependent oligomerization pathways regulate self-assembly of the periplasmic protease-chaperone DegP. *Proc. Natl Acad. Sci. USA.* **118**, e2109732118 (2021).
22. Singh, S. K., Parveen, S., SaiSree, L. & Reddy, M. Regulated proteolysis of a cross-link-specific peptidoglycan hydrolase contributes to bacterial morphogenesis. *Proc. Natl Acad. Sci. USA.* **112**, 10956–10961 (2015).
23. Razew, A. et al. Monitoring drug-protein interactions in the bacterial periplasm by solution nuclear magnetic resonance spectroscopy. *J. Am. Chem. Soc.* **146**, 9252–9260 (2024).
24. Robinson, K. E., Reardon, P. N. & Spicer, L. D. In-cell NMR spectroscopy in *Escherichia coli*. *Methods Mol. Biol.* **831**, 261–277 (2012).
25. Limatola, A. et al. Time-Resolved nmr analysis of proteolytic alpha-synuclein processing in vitro and in cellulo. *Proteomics* **18**, e1800056 (2018).
26. Bertini, I. et al. Mapping protein-protein interaction by 13C'-detected heteronuclear NMR spectroscopy. *J. Biomol. NMR* **36**, 111–122 (2006).
27. Pontoriero, L. et al. Monitoring the Interaction of alpha-Synuclein with Calcium Ions through Exclusively Heteronuclear Nuclear Magnetic Resonance Experiments. *Angew. Chem. Int. Ed. Engl.* **59**, 18537–18545 (2020).
28. Felli, I. C. & Pierattelli, R. (13)C Direct Detected NMR for Challenging Systems. *Chem. Rev.* **122**, 9468–9496 (2022).
29. Arunmanee, W. et al. Gram-negative trimeric porins have specific LPS binding sites that are essential for porin biogenesis. *Proc. Natl Acad. Sci. USA.* **113**, E5034–E5043 (2016).
30. Binolfi, A. et al. Intracellular repair of oxidation-damaged alpha-synuclein fails to target C-terminal modification sites. *Nat. Commun.* **7**, 10251 (2016).
31. O'Grady, C. et al. One-step amino acid selective isotope labeling of proteins in prototrophic *Escherichia coli* strains. *Anal. Biochem.* **426**, 126–128 (2012).
32. Jumper, J. et al. Highly accurate protein structure prediction with AlphaFold. *Nature* **596**, 583–589 (2021).
33. Songyang, Z. et al. Recognition of unique carboxyl-terminal motifs by distinct PDZ domains. *Science* **275**, 73–77 (1997).
34. Silber, K. R., Keiler, K. C. & Sauer, R. T. Tsp: a tail-specific protease that selectively degrades proteins with nonpolar C termini. *Proc. Natl Acad. Sci. USA.* **89**, 295–299 (1992).
35. Keiler, K. C. et al. C-terminal specific protein degradation: activity and substrate specificity of the Tsp protease. *Protein Sci.* **4**, 1507–1515 (1995).
36. Keiler, K. C. & Sauer, R. T. Sequence determinants of C-terminal substrate recognition by the Tsp protease. *J. Biol. Chem.* **271**, 2589–2593 (1996).
37. Keiler, K. C., Waller, P. R. & Sauer, R. T. Role of a peptide tagging system in degradation of proteins synthesized from damaged messenger RNA. *Science* **271**, 990–993 (1996).
38. Chueh, C. K. et al. Structural basis for the differential regulatory roles of the PDZ domain in C-terminal processing proteases. *mBio* **10**, e01129–19 (2019).
39. Su, M. Y. et al. Structural basis of adaptor-mediated protein degradation by the tail-specific PDZ-protease Prc. *Nat. Commun.* **8**, 1516 (2017).
40. Wang, S. et al. Structural basis for recruitment of peptidoglycan endopeptidase MepS by lipoprotein NlpI. *Nat. Commun.* **15**, 5461 (2024).
41. Nagasawa, H. et al. Determination of the cleavage site involved in C-terminal processing of penicillin-binding protein 3 of *Escherichia coli*. *J. Bacteriol.* **171**, 5890–5893 (1989).
42. Sauvage, E. et al. Crystal structure of penicillin-binding protein 3 (PBP3) from *Escherichia coli*. *PloS One* **9**, e98042 (2014).
43. Sambrook J. & D, R. *Molecular Cloning: A Laboratory Manual*. 3rd edn, Vol. 1 (Cold Spring Harbor Laboratory Press, 2001).
44. Datsenko, K. A. & Wanner, B. L. One-step inactivation of chromosomal genes in *Escherichia coli* K-12 using PCR products. *Proc. Natl Acad. Sci. USA.* **97**, 6640–6645 (2000).
45. Schneider, C. A., Rasband, W. S. & Eliceiri, K. W. NIH Image to ImageJ: 25 years of image analysis. *Nat. Methods* **9**, 671–675 (2012).
46. Osborn, M. J. & Munson, R. Separation of the inner (cytoplasmic) and outer membranes of Gram-negative bacteria. *Methods Enzymol.* **31**, 642–653 (1974).
47. Perez-Riverol, Y. et al. The PRIDE database at 20 years: 2025 update. *Nucleic Acids Res.* **53**, D543–D553 (2025).
48. Mirdita, M. et al. ColabFold: making protein folding accessible to all. *Nat. Methods* **19**, 679–682 (2022).

49. Hwang, T. L. & Shaka, A. J. Water suppression that works. Excitation sculpting using arbitrary wave-forms and pulsed-field gradients. *J. Magn. Reson.* **112**, 275–279 (1998).
50. Pervushin, K., Vogeli, B. & Eletsky, A. Longitudinal (1)H relaxation optimization in TROSY NMR spectroscopy. *J. Am. Chem. Soc.* **124**, 12898–12902 (2002).
51. Schanda, P., Kupce, E. & Brutscher, B. SOFAST-HMQC experiments for recording two-dimensional heteronuclear correlation spectra of proteins within a few seconds. *J. Biomol. NMR* **33**, 199–211 (2005).
52. Wu, D. H. & Chen, A. D. An Improved diffusion-ordered spectroscopy experiment incorporating bipolar-gradient pulses. *J. Mag. Res. A* **115**, 260–264 (1995). & S., J. C.
53. Kandiyal, P. S., Kim, J. Y., Fortunati, D. L. & Mok, K. H. Size Determination of protein oligomers/aggregates using diffusion nmr spectroscopy. *Methods Mol. Biol.* **2039**, 173–183 (2019).
54. Bermel, W. et al. Complete assignment of heteronuclear protein resonances by protonless NMR spectroscopy. *Angew. Chem. Int. Ed. Engl.* **44**, 3089–3092 (2005).
55. Gil, S. et al. NMR spectroscopic studies of intrinsically disordered proteins at near-physiological conditions. *Angew. Chem. Int. Ed. Engl.* **52**, 11808–11812 (2013).
56. Mori, S., Abeygunawardana, C., Johnson, M. O. & van Zijl, P. C. Improved sensitivity of HSQC spectra of exchanging protons at short interscan delays using a new fast HSQC (FHSQC) detection scheme that avoids water saturation. *J. Magn. Reson. B* **108**, 94–98 (1995).
57. Viennet T. et al. Decoding atomic addresses: solution NMR resonance assignment of proteins. in *Integrated Structural Biology - New Developments in NMR* (ed Quinn, C. M., Polenova, T. & Gronenborn, A. M.) Ch. 1, 1–42 https://doi.org/10.1039/BK9781837670154-00001 (Royal Society of Chemistry, 2023).
58. Lee, W., Tonelli, M. & Markley, J. L. NMRFAM-SPARKY: enhanced software for biomolecular NMR spectroscopy. *Bioinformatics* **31**, 1325–1327 (2015).


## Acknowledgements

This research was supported by a cooperation grant from MAECI (Italy) – MincyT (Argentina) to R.P. and A.J.V., grants from ASaCTeI (PEICID 2023-191 to A.J.V.), Subsecretaría de Ciencia y Tecnología de la Nación (REPARA, to A.J.V.), The Richard Lounsbery Foundation (2022-2024 to A.B.), Agencia I + D + i to A.J.V. (PICT 2020-0031 and PICT 2022-01-2022), L.J.G. (PICT 2020-1923) and A.B. (PICT 2018-02572). The support of the European Union-NextGenerationEU through the ItaliaDomani PNRR project "Potentiating the Italian Capacity for Structural Biology Services in Instruct-ERIC" (ITACA.SB, no. IR0000009) and of the Italian Ministry of Health project "Hub multidisciplinare e interregionale di ricerca e sperimentazione clinica per il contrasto alle pandemie ed all'antibiotico resistenza" (PAN-HUB 2021-T4-AN-07) to R.P. is gratefully acknowledged. Further support has been provided by iNEXT-Discovery (871037), funded by the Horizon 2020 program of the EC at the CERM/CIRMMP center of Instruct-ERIC. We thank Fernando Pasterán from Administración Nacional de Laboratorios e Institutos de Salud; Dr. C.G. Malbran", Argentina (ANLIS-Malbran) for providing the clinical strains. We also thank Fernando Soncini, Javier Palatnik, Diego de Mendoza, Enrico Luchinat and François-Xavier Theillet for reading the manuscript and providing feedback and Marina Avecilla and Enrique Morales for their technical assistance. Mass spectrometry instrument was from UEM-IBR. We thank Dr. Germán Rosano and Alejo Cantoia for the support and helpful discussions about mass spectrometry data. The NMR instrumentation at IBR was provided by PLABEM. We thank Lic. Andrea Coscia and Alejandro Gago for maintenance of the NMR infrastructure. F.J.H. is recipient of a postdoctoral fellowship from CONICET. A.J.V., A.B., and L.J.G. are staff members from CONICET.

## Author contributions

L.J.G., R.P., A.B., and A.J.V. crafted the main hypothesis and designed research. L.J.G. performed microbiological, molecular biology and biochemical experiments. L.J.G., L.P., R.P., A.B., and A.J.V. performed the NMR experiments. F.J.H. performed biochemical and confocal microscopy experiments. L.J.G., R.P., A.B., and A.J.V. wrote the paper, and all authors discussed the results and commented on the manuscript.

## Competing interests

The authors declare no competing interests.

## Additional information

**Supplementary information** The online version contains supplementary material available at https://doi.org/10.1038/s41467-025-62340-6.

**Correspondence** and requests for materials should be addressed to Lisandro J. González, Roberta Pierattelli, Andres Binolfi or Alejandro J. Vila.

**Peer review information** *Nature Communications* thanks Björn Burmann, Chung-I Chang and the other, anonymous, reviewer for their contribution to the peer review of this work. A peer review file is available.

**Reprints and permissions information** is available at http://www.nature.com/reprints

**Publisher's note** Springer Nature remains neutral with regard to jurisdictional claims in published maps and institutional affiliations.

**Open Access** This article is licensed under a Creative Commons Attribution-NonCommercial-NoDerivatives 4.0 International License, which permits any non-commercial use, sharing, distribution and reproduction in any medium or format, as long as you give appropriate credit to the original author(s) and the source, provide a link to the Creative Commons licence, and indicate if you modified the licensed material. You do not have permission under this licence to share adapted material derived from this article or parts of it. The images or other third party material in this article are included in the article's Creative Commons licence, unless indicated otherwise in a credit line to the material. If material is not included in the article's Creative Commons licence and your intended use is not permitted by statutory regulation or exceeds the permitted use, you will need to obtain permission directly from the copyright holder. To view a copy of this licence, visit http://creativecommons.org/licenses/by-nc-nd/4.0/.

© The Author(s) 2025